JPE 17-2-15

https://doi.org/10.6113/JPE.2017.17.2.464
ISSN(Print): 1598-2092 / ISSN(Online): 2093-4718

Output Voltage Regulation for Harmonic Compensation under Islanded Mode of Microgrid

Kyungbae Lim* and Jaeho Choi†

*,†School of Electrical Engineering, Chungbuk National University, Cheongju, Korea

Abstract

This study examines a P+multi resonant-based voltage control for voltage harmonics compensation under the islanded mode of a microgrid. In islanded mode, the inverter is defined as a voltage source to supply the full local load demand without the connection to the grid. On the other hand, the output voltage waveform is distorted by the negative and zero sequence components and current harmonics due to the unbalanced and nonlinear loads. In this paper, the P+multi resonant controller is used to compensate for the voltage harmonics. The gain tuning method is assessed by the tendency analysis of the controller as the variation of gain. In addition, this study analyzes the slight voltage magnitude drop due to the practical form of the P+multi resonant and proposes a counter method to solve this problem by adding the PI-based voltage restoration method. The proposed P+multi resonant controller to compensate for the voltage harmonics is verified through the PSIM simulation and experimental results.

Key words: Harmonics compensation, Islanded mode, PR control, Voltage control

I. INTRODUCTION

A microgrid is an integration of a RESs (renewable energy sources), such as photovoltaic or wind power generators and fuel cells, with engine generators, batteries, etc. that has been applied because of its flexibility and capability as a reliable power supply [1]-[6]. Therefore, the DG (distributed generation) based inverter, which is one of main equipment in a microgrid, has also been used.

Normally, the DG based inverter is defined as a current source in grid-connected mode [7]. In this mode, the attenuation of the current harmonics is possible by installing a L or LCL filter at the inverter output. On the other hand, a grid-connected inverter with a L or LCL filter needs to operate instantly as a voltage source after being disconnected from the main grid due to grid faults or strategic islanding [8]. In islanded mode, the inverter is defined as a voltage source to supply the full local load demand in place of the main grid. For the islanded mode of the inverter, however, the system modeling can be varied according to the location of the local load. Fig. 1 shows the grid-interactive inverter with a LCL filter, which has a local load. The local load can be located before or after the grid side inductor (L_g). If the local load is located between L_g and grid, it increases the system impedance due to the injection of L_g into system modeling. This increase in impedance can sometimes cause degradation of the control response. (Note that lower and higher output impedance have an advantage for the voltage and current control, respectively). In addition, the load voltage regulation also can be distorted due to the voltage drop of L_g. This is because the voltage sensing of the filter capacitor is common instead of sensing the load voltage in the case of a grid-interactive inverter. In this regard, the sine and cosine tables and the vector diagram-based capacitor voltage reference calculation method was proposed for the load voltage power quality in [9], [10] when the load is located on the output of the LCL filter. Nevertheless, this method for maintaining the load voltage quality is still difficult to implement, particularly when the inverter supplies a nonlinear load. Therefore, the local load location in this paper has been considered as the output of the LC filter to avoid not only increasing the impedance but also the complexity of modeling for voltage control under islanded mode.

The ultimate aim of inverter voltage control with a LC filter is to maintain the robustness and reliability for the regulation of the output voltage; however, there are some limitations in meeting the output voltage regulation [7].

Manuscript received Oct. 6, 2016; accepted Feb. 5, 2017
Recommended for publication by Associate Editor Rae-Young Kim.
†Corresponding Author: choi@cbnu.ac.kr
Tel: +82-43-261-2425, Fax: +82-43-276-7217, Chungbuk Nat'l Univ.
*School of Electrical Eng., Chungbuk National University, Korea

Firstly, its fast and robust voltage control are not guaranteed due to the non-zero output impedance characteristics of the output LC filter [7], even though the output impedance of the LC filter is smaller than the impedance of the LCL filter. Secondly, because the local load is located at the inverter output, which is composed mainly of nonlinear loads or occasionally unbalanced loads, it can cause the distortion of the output voltage, which affects the voltage regulation and the life span of the critical loads [7], [11], [12]. This is because local loads fed from an AC inverter generate the current harmonics if they are nonlinear loads and the negative and the zero sequence harmonics if an unbalanced component also occurs.

To solve the abovementioned problems, there have been several studies on multi-looped controllers, which can achieve the fast dynamic response or harmonics compensation possible despite the inverter output filter [7], [8], [11]-[17]. The double loop controller with an outer PI voltage loop and an inner P or PI current loop was introduced for the operation of a parallel UPS [13]. In [14], the PI-based voltage control, which included the harmonics compensation term, was proposed. This also guaranteed the transient dynamics using the inner current feedforward term instead of the inner current loop. The nonlinear and unbalanced components caused by local loads were compensated for [14]. On the other hand, the harmonics compensation using PI control is quite complicated because it requires a band-pass filter and PLLs (phase-locked loops) for each harmonic frequency. In addition, it cannot control the positive and negative sequences simultaneously using only one controller [18]. To avoid this complexity, the PR (P+resonant) based output voltage controllers, which can control both the positive and negative sequences simultaneously, were considered [11], [12], [15]-[19]. References [15], [16], [19] describe its characteristics and how the PR control can be possible under a stationary reference frame. In [11], [12], [17], the P+multi resonant (P+MR) controller (Fig. 2) has been selected with a multi-loop topology for the regulation of voltage control and analyzed the performance of voltage regulation to meet the rapid dynamics and harmonics compensation under the nonlinear and unbalanced load conditions. However, it is neglected how to design parameters of the PR controller and its specific control characteristics. In [7], [8], the P+MR control was selected with the specific system modeling to determine the gain parameters properly. On the other hand, its system analysis was insufficient to understand the various response tendencies according to each control gain variation. In addition, the voltage magnitude tracking had a steady-state magnitude error because it used the practical form of PR control which added a low pass term to the ideal PR control [19].

In this paper, the P+MR based multi loop control

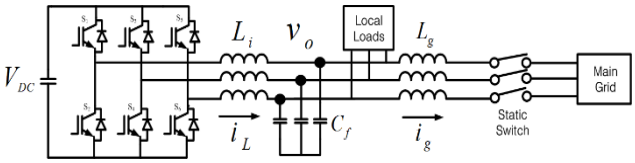

Fig. 1. System configuration according to load location.

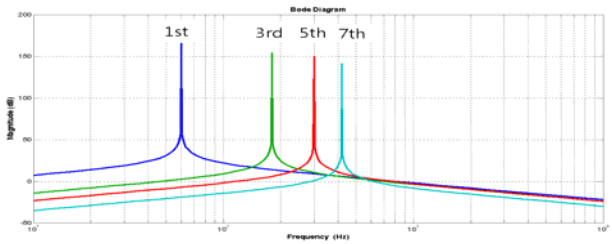

Fig. 2. Bode plot of P+MR voltage controller.

coordinated in αβ- and abc-frames is selected to compensate for the voltage harmonics with a rapid dynamic response referred in [7], [8]. The controller gains based on specific modeling are tuned using the bode plot and root locus.

Unlike [7], [8], changes of each control gain are added under the root locus-based control gain selection criteria to analyze the characteristics of each gain and mutual influence. This analysis is extended to the Bode plot-based P+MR term to make gain optimizing be possible to handle the unexpected variable occurrences, such as system parameter mismatch, etc. In addition, the simple PI-based magnitude restoration term is added by modifying the voltage reference adaptively to maintain the regulated voltage magnitude as its rated value in islanded mode, because the regulated output voltage magnitude error can occur by decreasing the control gain due to the use of practical PR control, which includes the low-pass term.

Finally, the proposed algorithm for the P+MR resonant compensation is verified and it is concluded that their proper gain selection and voltage restoration method can guarantee the output voltage quality with simple implementation through a comparison with the PI-based harmonic compensation method. For the verification, PSIM simulations are applied for a 90kW inverter and a 600W laboratory scaled setup is used for experiments.

II. Controller Design

The P+MR controller is used to compensate for the harmonic components in this paper. The controller is composed of an outer P+MR voltage control loop and an inner proportional current control loop for zero steady-state error and enhancing the system transient dynamic, respectively. As mentioned in section I already, this paper proposes how to select the gain parameters. The gain selection sequence can be summarized as followings:

1) The inner current proportional gain, K_{c_p}, must be

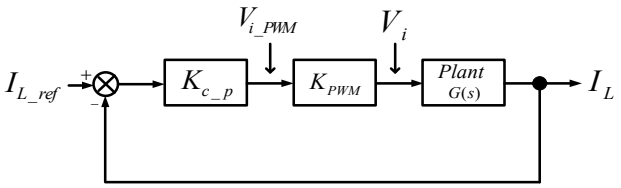

Fig. 3. Block diagram of inner current control loop.

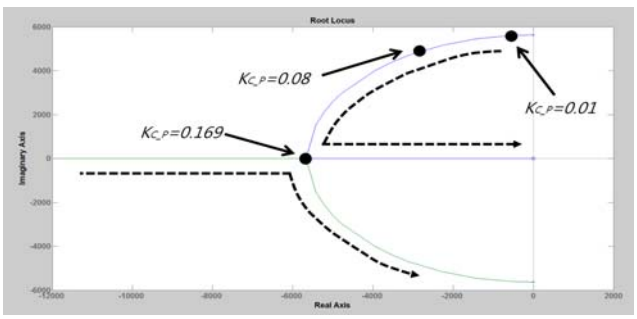

Fig. 4. Root locus of current control loop with various K_{c_p}.

selected firstly to realize the fully LC resonance damping.

2) The cut-off frequency, $\omega_{n.cut}$, has to be designed after considering the available operating frequency boundary.
3) The proportional voltage loop gain, K_p, can be selected to meet the proper damping ratio for the transient dynamic response. As mentioned in many PR related researches, the transient dynamic response can be affected by K_p.
4) The resonant gain variation-based root locus has to be considered with '0' value of K_p. Here, the operator has to select any resonant gain values which satisfy '1' damping ratio. Therefore, the selected fundamental resonant gain value rarely affects the transient dynamic. And then the harmonic resonant gain can be obtained by adding the harmonic resonant control term to the PR control characteristic equation compromising between the control performance and the system stability.

A. Design of Voltage Controller with Inner Current Control Loop

Fig. 3 presents a block diagram of the inner current controller. Here, K_{c_p} and K_{pwm} represent the proportional gain of the current controller and the PWM gain, respectively. *G(s)* represents the LC filter transfer function when the output current, I_o, is assumed as a disturbance. On this, *G(s)* can be written as follows:

$$G(s)=\frac{I_L(s)}{V_i(s)}=\frac{sC}{s^2LC+1} \tag{1}$$

Substituting equation (1) into Fig. 3 gives

$$\frac{I_L(s)}{I_{L\_ref}(s)}=\frac{sK_{c\_p}K_{PWM}C_f}{s^2L_iC_f+sK_{c\_p}K_{PWM}C_f+1} \tag{2}$$

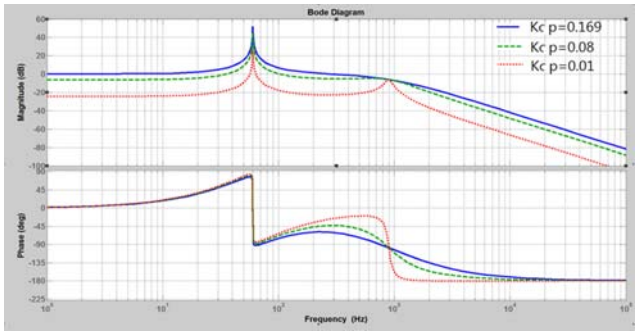

Fig. 5. Bode plots of open loop transfer function of voltage control loop with different K_{c_p}.

Fig. 4 shows the root locus from equation (2) according to various K_{c_p} when K_{pwm} is assumed to be '1' [11]. As shown in this figure, all oscillation characteristics can be eliminated entirely for $K_{c\_p} \geq 0.17$. Fig. 5 shows the Bode plots of the transfer function of the open loop voltage controller with different values of K_{c_p} derived from Fig. 4. As shown in this figure, all resonant oscillations are eliminated when K_{c_p} is over 0.17, but the resonance oscillation becomes serious at the LC resonant frequency when K_{c_p} changes from 0.169 to 0.01. The control action can be decreased as the entire gains of the other frequencies become lower, and it would be more unstable, which becomes closer to the threshold value, -180°. This means that the system can be unstable due to the considerable resonance at the LC resonant frequency. Therefore, K_{c_p} is selected as 0.17, which satisfies the elimination of all oscillations and the minimum bandwidth of the controller. In other words, all oscillation elimination and proper control margins can be guaranteed with this value. Equation (3) is used for voltage control.

$$H_{PMR} \Rightarrow K_P+\frac{K_i\omega_{1.cut}s}{s^2+2\omega_{1.cut}s+\omega_o^2} + \sum_{n=3,5,7th}\frac{K_{in}\omega_{n.cut}s}{s^2+2\omega_{n.cut}s+(n\omega_o)^2} \tag{3}$$

Equation (3) is the transferred stationary term from PI control under a synchronous dq frame. The equation includes a low pass filter to make the ideal PR control more practical. Therefore, it is more robust for small frequency changes. Equation (3) also includes a 's' term in the nominator of resonant controller, so it has a larger phase margin and guarantees better dynamic performance than that without the 's' term [19], [20]. Here, $K_{i,1}\omega_{1,cut}$ is the resonant gain of voltage controller for n^{th} frequency. As shown in Fig. 2, the controller has large gain on the frequencies at each order of harmonics to compensate for the harmonics generated from the unbalanced and nonlinear loads. Therefore, the 1, 3, 5, and 7^{th} harmonics can be compensated by P+MR voltage controller under the islanded mode. In this paper, the inner proportional current controller is added to enhance the aforementioned system transient dynamic, as shown in Fig. 6. On the other hand, the proportional current loop causes a significant phase

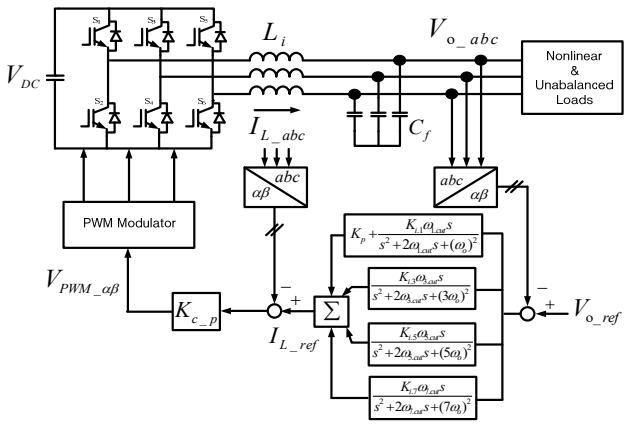

Fig. 6. Configuration of P+MR controller in islanded mode.

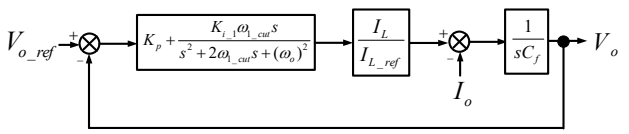

Fig. 7. Block diagram of outer voltage control loop.

shift at the operating frequency. Therefore, the large voltage loop controller gain is essential to compensate for the phase shift and ensure the negligible steady state error [11].

Fig. 7 shows the closed loop block diagram of fundamental component voltage control [7], [8], [11]. The closed loop transfer function can be obtained in common with the case of the inner current loop.

B. Design of Cut-Off Frequency, $\omega_{n,cut}$

When the inverter is operated under the grid-connected conditions, the inverter generates a current synchronized by the phase of the grid voltage. However, the grid frequency is not fixed correctly at 60Hz and may change within the operating frequency range in the steady state of grid-connected mode. Therefore, the ideal PR control with a fixed resonant frequency is unsuitable for the grid-connected mode control under a weak-grid which sometimes shows the fluctuation of the grid. These problems could be improved by using the PI control under a synchronous dq frame or the PR control with dynamic resonant frequency to synchronize adaptively the grid fluctuation [21], [22].

In the islanded mode operation of a microgrid, the voltage reference is fixed. Therefore, the output frequency changing problem under the islanded mode is not as serious as that in the grid-connected mode. This is because the frequency change under the islanded mode occurs intermittently within a stable operating frequency region. Although inverters use the droop control to share the output power by changing the frequency and magnitude intentionally, this changeable region of frequency is within the stable region by constant voltage and frequency by microprocessor. Therefore, in the islanded mode, the practical PR control form with $\omega_{n.cut}$ as shown in equation (3) is sufficient to meet the stable output voltage regulation for both transient and steady-state of islanded mode [19], [23].

The cut-off frequency for fundamental component, $\omega_{1,cut}$, and that for the harmonic frequency components, $\omega_{n,cut}$, can be designed using the following equations [7], [8]:

$$\zeta = \frac{\omega_{n.cut}}{n\omega_o} \tag{4}$$

$$\omega_{5.cut} = 5 \cdot \omega_{1.cut} \tag{5}$$

$$\omega_{7.cut} = 7 \cdot \omega_{1.cut} \tag{6}$$

From equation (3), the damping factor, ζ, and the cutoff frequencies of the PR controller are defined by equations (4) to (6). In this paper, the fundamental cutoff frequency $\omega_{1.cut}$ has been designed to cover ±1% of frequency offset. Therefore, $\omega_{1.cut}$ can be designed as $\omega_{1.cut} = 2\times\pi\times60\times1\% \approx 3.769 \approx 4$ rad/s [24]. The cutoff frequencies of harmonic terms have been designed as equations (5) and (6), and they have to meet the same damping ratio for the cutoff frequencies of harmonic terms as that for the fundamental frequency.

C. Selection of PR Voltage Control Gain

To select the PR voltage gain, there was a study based on the entire closed loop transfer function of voltage control [8]. The resonant gain was assumed to be '0' and the proportional gain was selected when the damping ratio reached 0.707 by changing the proportional gain. The proper resonant gain was then selected through the root locus as the same method after assuming '0' proportional gain. On the other hand, this method was not enough to verify that the system dynamic response is dependent mainly on the proportional gain. In addition, it could not cover the error due to the mismatch of the plant parameters, because this research was carried out without tendency analysis according to the variation of each gain. Therefore, in this paper, as extended from gain selection method of [8], the tendency according to each gain and the mutual influence of gains have been analyzed through both the proportional gain sweep-based root locus with different resonant gain and resonant gain sweep-based root locus with different proportional gains.

Fig. 8 shows the root locus with the variation of resonant gain for the different proportional gain. As shown in this figure, the root moves to the direction of the right half plane with increasing resonant gain. ① in Fig. 8 is the root locus when the proportional gain is as '0'.

Here, considering the unexpected parameter mismatch, the resonant gain in this paper has been selected as 4660 within the resonant gain values, which makes the damping ratio '1' based on the ① root locus. The locus variation from ① to ④ has the same directional nature with a proportional gain increase and their damping ratio decreases at the point with the '0' resonant gain values. This means that the more system dynamic response can be improved, the larger proportional

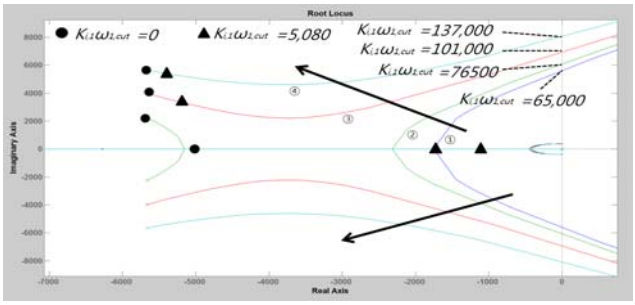

Fig. 8. Root locus with variation of $K_{i,1}\omega_{1,cut}$ for different K_p. (Arrow direction indicates increasing K_p: ① 0, ② 1, ③ 3, ④ 6)

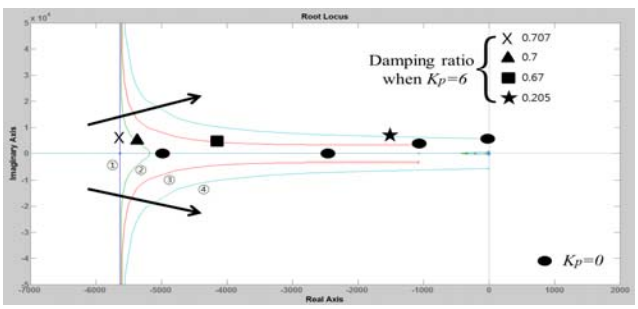

Fig. 9. Root locus with variation of K_p for different $K_{i,1}\omega_{1,cut}$. (Arrow direction indicates increasing of $K_{i,1}\omega_{1,cut}$:① 0, ② 4660, ③ 20000, ④ 60000)

gain is. Furthermore, as shown from the point where the horizontal axis is '0', the resonant gain of the system instability critical point increases with increasing proportional gain. In other words, under the same resonant gain, the phase margin will be boosted at the crossover frequency under the PR voltage control transfer function-based bode plot. On the other hand, an excessive increase in proportional gain is not preferred due to the limited switching frequency. Therefore, the proportional gain selection needs to be carried out considering the tradeoff between the sufficient control margin and dynamic response.

Fig. 9 shows the proportional gain variation-based root locus under different resonant gains. In common with Fig. 8, the proportional gain increases with decreasing the system damping ratio. The arrow direction indicates the increase of the resonant gain and each point (dot), which has the same proportional gain, moves to almost to the right half plane and their y-axis value is not changed significantly compared to the changes in the x-axis. In other words, the increase in resonant gain is related to the y-axis of the root locus, which results in the system dynamic response, but it is very little compared to the proportional gain changes to the dynamic response. This means that an increase in resonant gain decreases the phase margin on the crossover frequency with the same proportional gain. Therefore, an increase in resonant gain can improve the control performance under a steady-state and can cause system instability due to the decrease in phase margin. Therefore, the resonant gain needs

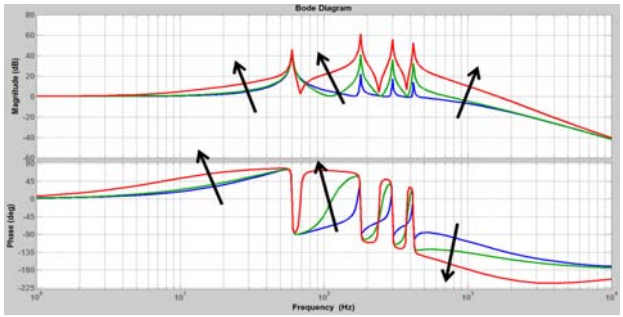

Fig. 10. Bode plot of voltage controller with harmonics compensation: K_p=6, $K_{i.3,5,7}\cdot\omega_{3,5,7.cut}$=$8\times10^2$, 8×10^3, 8×10^4. (arrow direction indicates increasing value of $K_{i.3,5,7}\cdot\omega_{3,5,7.cut}$)

to be selected after compromising between the phase margin for stability and the control performance under the steady state.

Finally, it is verified that the dynamic response of the PR voltage control is affected mainly by the proportional gain. Therefore, in this paper, the proportional gain has been selected as 6, of which the system damping ratio satisfies 0.707 when the resonant gain is '0' as shown in Fig. 9.

This can be extended to harmonics compensation. Fig. 10 shows the bode plot of the open loop transfer function of the voltage controller for harmonics compensation with various resonant gains. The vertical line represents each harmonic frequency. From this figure, the proper harmonic resonant gain can be obtained with the appropriate phase and gain margins. Otherwise, it can cause the system instability, leading to system oscillation. If it has lower resonant gain, the ability of harmonics compensation will decrease in proportion to the resonant gain value. Each harmonics resonant gain may be different according to the amount of each harmonic or strategic tuning of the phase margin to satisfy the system stability.

For more detailed system analysis, the proportional gain, K_p, and inner current loop proportional gain, K_{c_p}, of the voltage controller is varied in Figs. 11 and 12, respectively. As shown in Fig. 11, the proportional gain of the voltage controller affects the gain in all frequency ranges except for fundamental and harmonics frequency region, which is different from Fig. 10. In Fig. 10, the resonant gain variation only affects the fundamental and harmonic frequency region. This means that the voltage proportional gain variation affects mainly the transient dynamic and does not affect the steady state voltage regulation. On the other hand, the resonant gain variation only affects the steady state voltage regulation and phase margin. Fig. 12 shows the bode plot of the voltage control when the inner current loop proportional gain varies. Here, the inner current loop gain, K_{c_p}, variation affects the gain at the fundamental and harmonic frequencies. Therefore, it also affects the dynamic characteristics and the steady state voltage regulation performance. Hence, it is important to design the system modeling with the correct parameter as well as to consider the all frequency factors, such as the LC resonance, control bandwidth, the crossover frequency and the switching

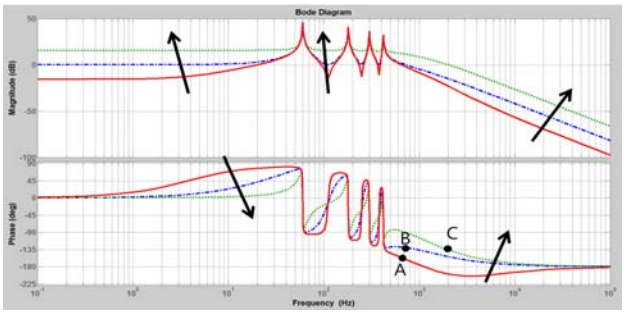

Fig. 11. Bode plot of voltage controller with harmonics compensation: K_p=1, 6, 36, $K_{i.3,5,7}\cdot\omega_{3,5,7.cut}=8\times10^3$. (arrow direction indicates increasing value of K_p)

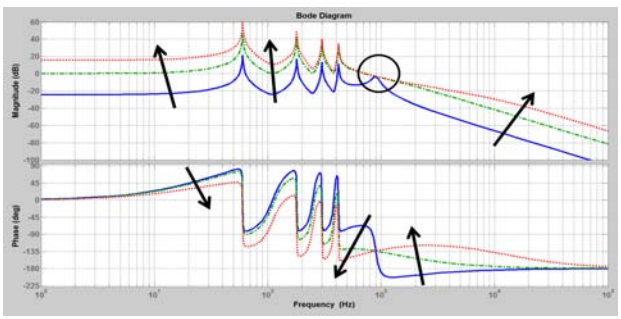

Fig. 12. Bode plot of voltage controller with harmonics compensation: K_p=6, $K_{i.3,5,7}\cdot\omega_{3,5,7.cut}= 8\times10^3$, K_{c_p}=0.01, 0.17, 1. (arrow direction indicates increasing value of K_{c_p})

frequency, etc.

D. Proposed Restoration Method for Voltage Regulation

Fig. 13 shows the effect of the proposed method for the d-axis component of the output load voltage, which represents the magnitude information in islanded mode. The magnitude of output load voltage is decreased with the conventional voltage reference, V_{ref}. This is caused mainly by using the practical PR control (solid line) in Fig. 14. As shown in this figure, the ideal PR control (dot line) is quite sensitive to the frequency variation because it has the very overlarge gain within a narrow frequency band. Therefore, the practical PR control achieved by combining with the low-pass filter can be adopted to supplement the disadvantage of the ideal PR control. This practical PR control, however, causes incorrect tracking of the rated voltage magnitude due to the decrease in the control gain magnitude at the center frequency, 60Hz, as shown in Fig. 14. (Note that this characteristics due to the decrease of gain on the center frequency does not affect the rated voltage tracking under the grid-connected mode because the output current PR controller autonomously can regulate the output voltage to supply the reference current to the grid of which the equivalent impedance is relatively small under the grid-connected mode.) Therefore, the modified method for generating the reference output voltage using a low pass filter is proposed to maintain the output voltage as a rated value adaptively. The proposed method is modeled to be effective

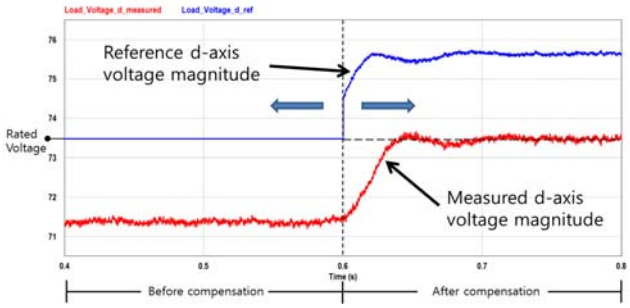

Fig. 13. Simulation result of d-axis of load voltage under islanded mode with conventional and proposed voltage reference.

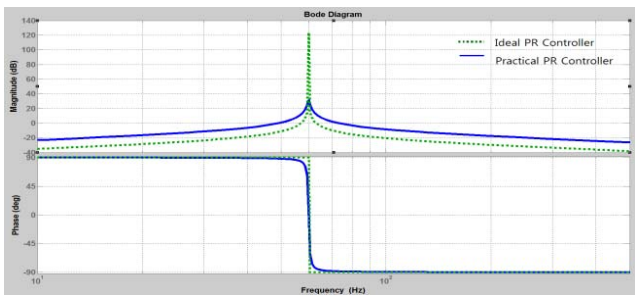

Fig. 14. Bode plot of ideal and practical PR controller.

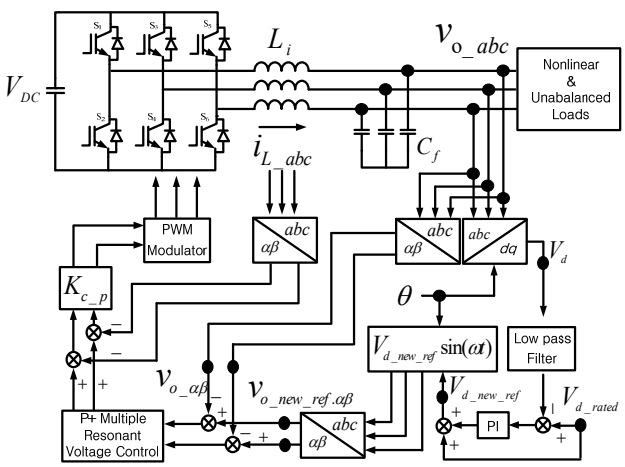

Fig. 15. Proposed whole control scheme with implementation of voltage restoration.

just under the islanded mode, and it can be carried out by adding the PI control output of the voltage magnitude error to the conventional magnitude of the reference, as shown in Fig. 15. Therefore, with the new voltage reference obtained from the proposed control algorithm, the d-axis component of the output load voltage is improved as shown after 0.6s in Fig. 13.

In addition, the other gain attenuation issue occurs under the grid connected mode due to the change of the grid frequency. In this case, the PR control with dynamic resonant frequency [21], [22] or P+ Lattice control [25], which has the

TABLE I
SIMULATION PARAMETER

Parameters			Value	Unit
Rated active power			90	kW
DC link voltage			158	V
Rated output voltage			73.4	V
Switching frequency			4	kHz
Filter capacitor, C_f			2100(Y),700(Δ)	μF
Inverter side inductor, L_i			15	μH
PI control gain	1st Controller	Voltage	1 , 500	Ω^{-1}
		Current	0.08, 16	Ω
	harmonic compensation		0.5 , 0.01	None
PR control gain	P gain(K_p), P gain (K_{c_p})		6 , 0.17	Ω^{-1}, Ω
	Resonant gain (1st)		4660	Ω^{-1}
	Resonant gain (3th)		8000	Ω^{-1}
	Resonant gain (5,7,11th)		8000	Ω^{-1}
	Cut-off Frequency		4,12, 20, 28,44	rad/s

different discretization and control form from the PR control, may be used to synchronize the grid fluctuation adaptively.

III. SIMULATION RESULTS

Table I lists the system parameters for the simulation. In this study, the performance of controllers to supply the sinusoidal output voltage under a nonlinear and unbalanced load is analyzed through the PSIM simulation.

Fig. 16 shows the conventional PI control performance supplying a nonlinear load without harmonics compensation. Fig. 16(a) shows the output voltage waveform distorted by the nonlinear load. Fig. 16(b) shows the result of FFT analysis of phase-A voltage and its THD is 15.2%. Fig. 17 presents the performance of PI control with 5th and 7th harmonics compensation. After harmonics compensation, the THD can be improved to 4.4%.

Fig. 18 shows the performance of P+MR control supplying a nonlinear load with the harmonics compensation method. The 5th and 7th harmonics are compensated well and the THD is 3.9%. The difference in the THD compensation performance in Figs. 17(b) and 18(b) can be reduced by changing each integral (I) of the PI controller and resonant (R) harmonic gain of the PR controller. In other words, the performance of harmonics compensation does not depend on the type of controller and it depends mainly on the size of the harmonics compensation gain. Fig. 19 represents the P+MR control performance supplying an unbalanced and nonlinear load with a 3rd harmonics compensation. As shown in Fig. 19(a) and (b), there is the 3rd harmonics before compensation, but it is eliminated after the compensation, as shown in Fig. 19(c) and (d) with a 4.4% THD. Fig. 20 shows the simulation results of the P+MR control performance with 0.01 $K_{c,p}$ which is less than the selected value of 0.17. As shown in this figure, the controller cannot eliminate the LC resonance effect, as mentioned in Figs. 5, 6, and 12. Therefore, the 17th harmonics component becomes very large because it is close to the LC

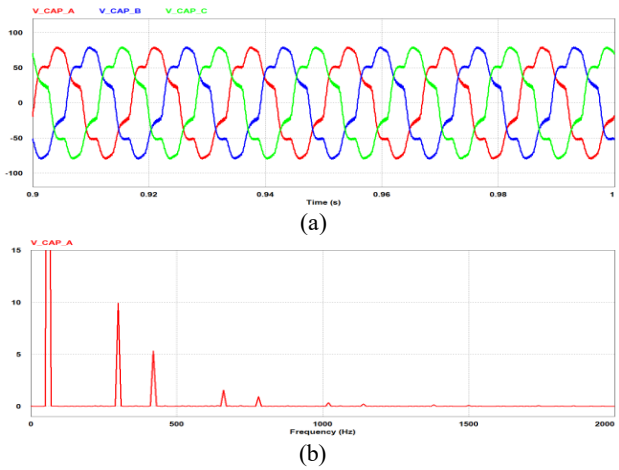

(a)
(b)

Fig. 16. Simulation results of PI control performance supplying non-linear load without harmonics compensation: (a) Output voltage waveforms, (b) FFT of output voltage. (THD: 15.2%).

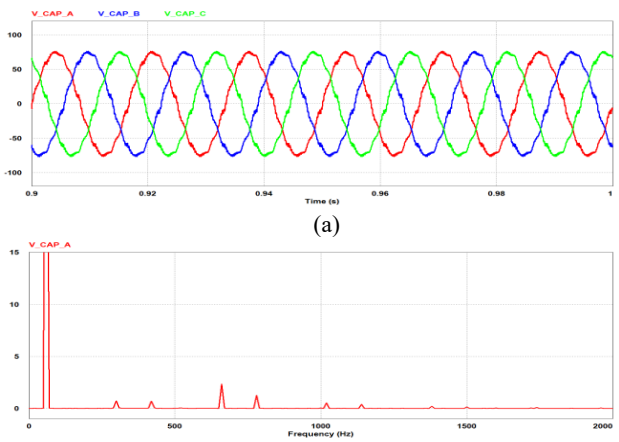

(a)
(b)

Fig. 17. Simulation results of PI control performance supplying non-linear load with 5th and 7th harmonics compensation: (a) Output voltage waveforms, (b) FFT of output voltage. (THD: 4.4%).

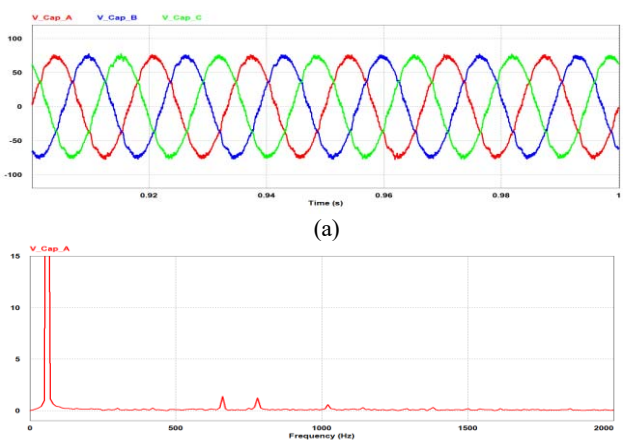

(a)
(b)

Fig. 18. Simulation results of P+MR control performance supplying non-linear load with 5th and 7th harmonics compensation: (a) Output voltage waveforms, (b) FFT of output voltage. (THD: 3.9%).

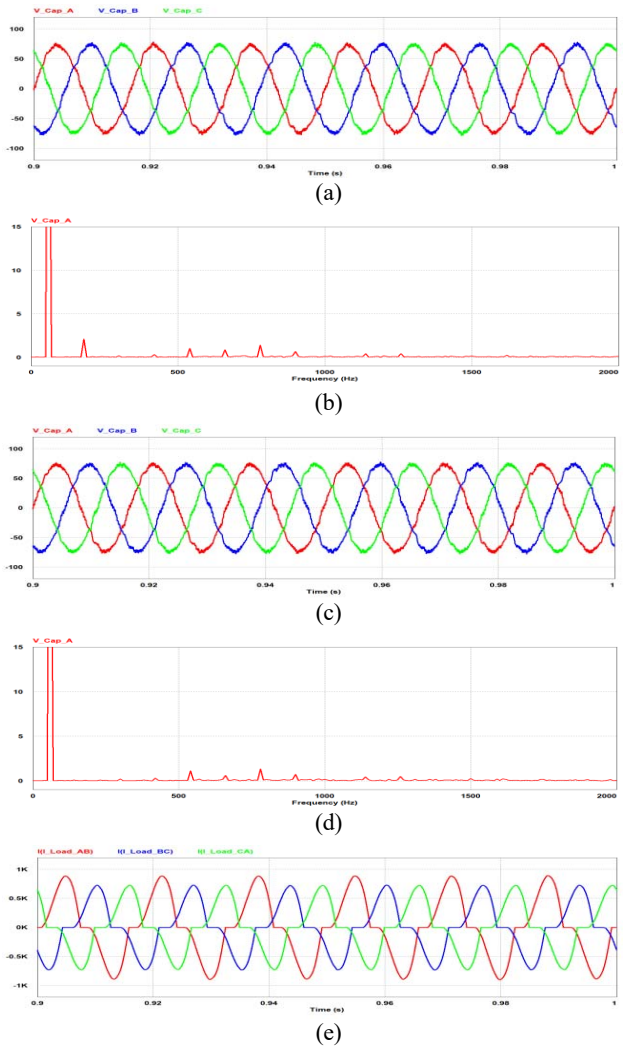

(a) (b) (c) (d) (e)

Fig. 19. Simulation results of P+MR control performance supplying unbalanced and non-linear load: (a) Output voltage waveforms with 5th and 7th harmonics compensation, (b) FFT of output voltage of (a) (THD: 4.9%), (c) output voltage waveforms with 3rd, 5th, 7th harmonics compensation, (d) FFT of output voltage of (c) (THD: 4.4%), (e) distorted unbalanced and nonlinear load current of (c).

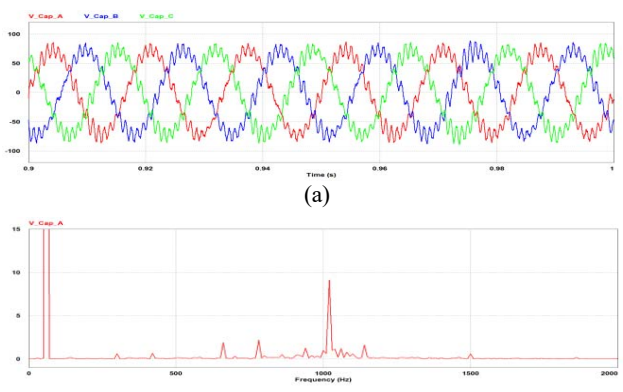

(a) (b)

Fig. 20. Simulation results of P+MR control performance supplying non-linear load with 0.01 $K_{c,p}$: (a) Output voltage waveform with 5th and 7th harmonics compensation, (b) FFT of output voltage. (THD: 14%)

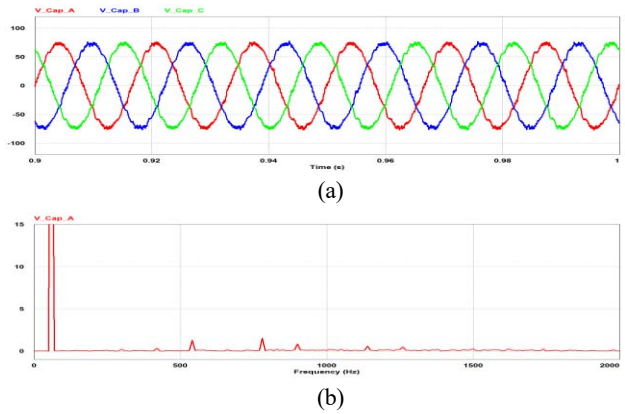

(a) (b)

Fig. 21. Simulation results of P+MR control performance supplying unbalanced and non-linear load: (a) Output voltage waveforms with a 3rd, 5th , 7th and 11th harmonics compensation, (b) FFT of output voltage of (a). (THD: 4.2%)

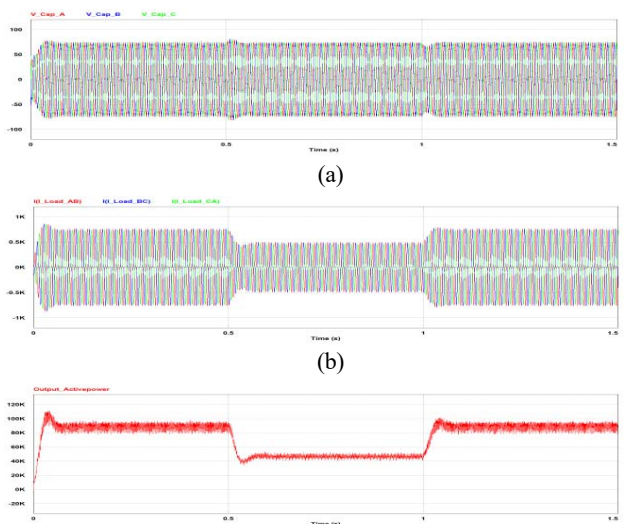

(a) (b) (c)

Fig. 22. Simulation results of P+MR control performance supplying unbalanced and non-linear load when load changes (90kW⟶45 kW⟶90kW): (a) Output voltage waveforms, (b) load current waveform, (c) output active power.

resonant frequency. In addition, 11th harmonics compensation term is also considered in Fig. 21. As shown in this figure, its THD compensating performance is improved comparing with that when only the 3rd, 5th, and 7th harmonics terms exist (THD: 4.4⟶4.2). This is because the 11th harmonics component has a small effect in the entire THD component initially and its phase margin by adding the 11th harmonics compensation term is 35°, which is lower than the 50° phase margin at which only the 3rd, 5th, and 7th harmonics terms are used, which represent slightly unstable system than before. Hence, the addition of the 11th or further 13th harmonics compensation term is needed under the compromise between the system stability and harmonics compensation performance.

Fig. 22 shows the output voltage, load current and output active power to analyze the transition response characteristics when an unbalanced and non-linear load changes from 90kW

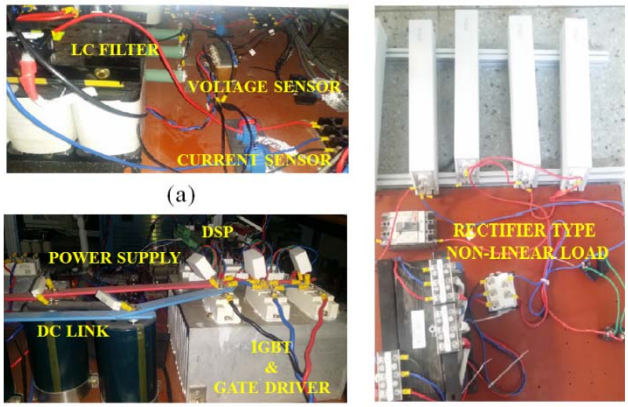

Fig. 23. Pictures of experimental setup: (a) LC filter and sensor part, (b) inverter IGBT stack and DSP part, (c) nonlinear load part.

TABLE II
EXPERIMENTAL PARAMETER

Parameters		Value	Unit
Rated active power		600	W
DC link voltage		400	Vdc
Rated output voltage		158	Vrms
Switching frequency		5	kHz
Filter capacitor, C_f		40(Y)	μF
Inverter side inductor, L_i		3	mH
PR control gain	P gain(K_p), P gain (K_{c_p})	0.0354 , 16	Ω^{-1}, Ω
	Resonant gain (1st)	30	Ω^{-1}
	Resonant gain (3th)	50	Ω^{-1}
	Resonant gain (5,7th)	50	Ω^{-1}
	Cut-off Frequency	4, 12, 20, 28	rad/s

to 45kW and from 45kW to 90kW at 0.5s and 1s, respectively. This figure shows that it reaches the steady-state with a rapid dynamics under the load changes. These results confirm that the gain selection under the criteria in this paper satisfies the stable transition response and the effective harmonic compensation.

IV. EXPERIMENTAL RESULTS

To investigate the proposed control strategy, an experimental setup has been established as shown in Fig. 23 and all parameters in experiments are shown in Table II. The controller gains in experiments are different from those in simulation, because LC values are different from each other due to the different power rating in simulations and experiments. Hence, the selected gains are also different, which are derived from the given LC values. Furthermore, after the gain selection, it has to be tuned a little considering the system condition, such as the parasitic resistance of LC components.

Fig. 24(a) presents the experimental results of the P+ fundamental R control performance supplying a non-linear

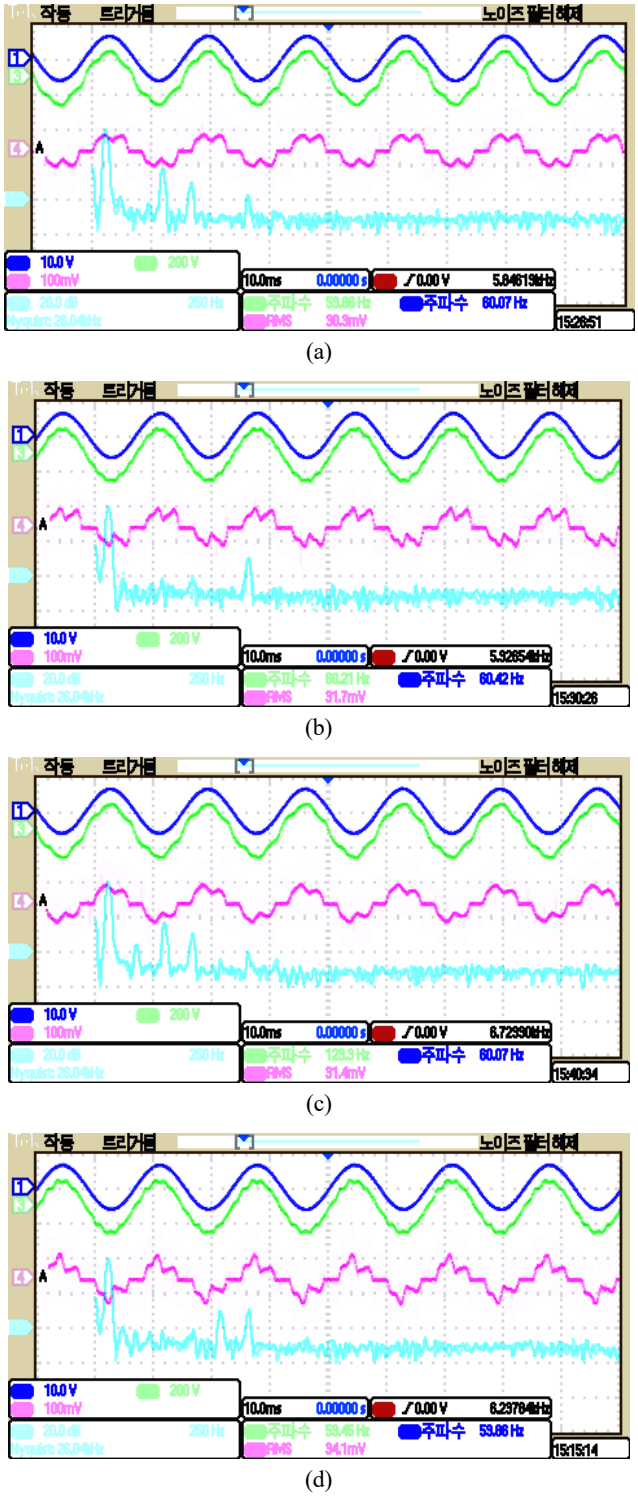

Fig. 24. Experimental results for phase A (From top to bottom: voltage reference waveform, measured output voltage waveform, output load current waveform, FFT of measured output voltage):
(a) P+fundamental R control performance supplying the non-linear load (THD: 8.5%), (b) P+MR control performance with 5^{th} and 7^{th} harmonics compensation supplying non-linear load (THD: 3.8%), (c) P+fundamental R control performance supplying unbalanced and non-linear load (THD: 9.1%), (d) P+MR control R performance with 3^{rd}, 5^{th}, and 7^{th} harmonics compensation supplying non-linear load. (THD: 4.3%).

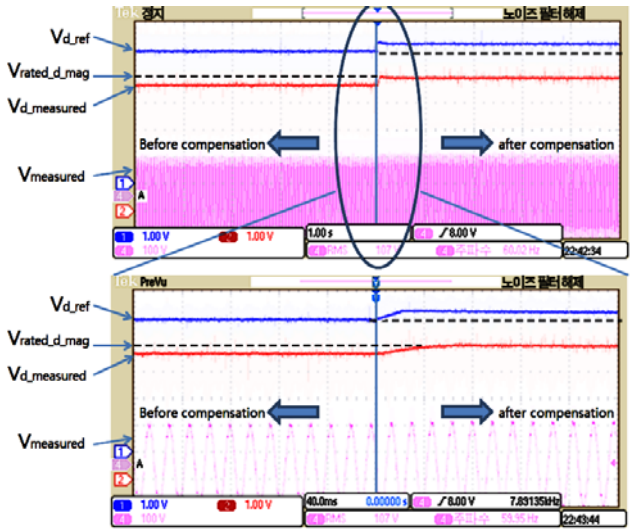

Fig. 25. Experimental results with or without voltage restoration method (From top to bottom: d-axis of output voltage reference, d-axis of measured output voltage, A phase measured output voltage, black-dot: d-axis of rated output voltage) (Top) zoomed out waveform (Bot) zoomed in waveform when voltage restoration starts.

load. As shown in this figure, it tracks the voltage reference magnitude well as the proposed voltage restoration technique. On the other hand, its measured output voltage waveform is distorted considerably because it does not apply the 5th and 7th harmonics compensation term. The load current waveform is also distorted because it supplies a nonlinear load. Its division is 1A/10mV. The bottom waveform shows the FFT results of the measured output voltage of which the division is 250Hz/div. As mentioned above, the 5th and 7th harmonics components appear due to the absence of a harmonics compensation term. Fig. 24(b) also presents the A phase experimental result of the P+MR performance supplying a non-linear load. Compared to Fig. 24(a), its voltage waveform has been improved to be more like a sinusoidal curve due to the presence of a harmonics compensation term (5th and 7th). In addition, it can be rechecked with a decrease in the 5th and 7th harmonics components, as shown in the FFT results. Fig. 24(c) shows the A phase experimental result of the P+fundamental R performance supplying an unbalanced and non-linear load. Compared to Fig. 24(a), its measured voltage THD is worse than that of Fig. 24(b) because of the appearance of the 3rd harmonic component due to the unbalancing factor into the loads (THD8.5⟶9.1%)). In addition, it can be also checked, as shown in the FFT results. Fig. 24(d) presents the A phase experimental result of the P+MR performance supplying an unbalanced and non-linear load. Compared to Fig. 24(c), its voltage waveform is improved to be more sinusoidal due to the presence of the harmonics compensation term (3rd, 5th, and 7th). On the other hand, its THD after harmonics compensation is worse than that in Fig. 24(b) because the 3rd harmonics and 9th harmonics, which is proportional to the 3rd harmonics, appeared at the same time.

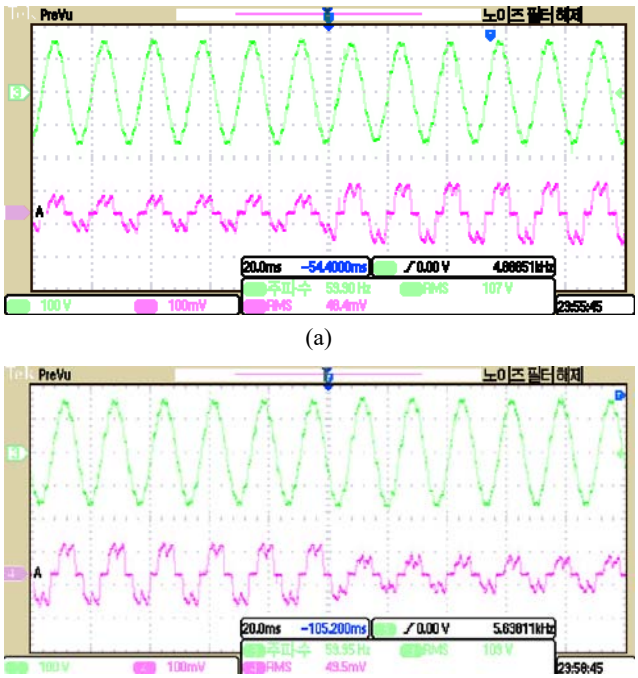

Fig. 26. Transient response of output voltage and current waveforms under load changes: (a) Increasing load, (b) decreasing load (Top: output voltage, bottom: output current).

Figure 25 shows the experimental results with or without the voltage restoration method. For an easier comparison, the d-axis of both the output voltage reference and measured output voltage has one division offset difference in the Y-axis. As shown in this figure, the d-axis of the measured value has the steady state error from the d-axis of the reference value before applying the voltage restoration method. On the other hand, after applying this method, the PI-based voltage restoration method changed its magnitude reference value adaptively to make the measured d-axis output voltage track its rated value. The d-axis of the measured output voltage tracks its rated value with an almost zero steady state error in 4 cycles. Therefore, the voltage restoration method is verified to realize the good magnitude tracking performance by the experimental results, too.

Fig. 26 represents the dynamic load transient waveform. As shown in above figures, the proposed PR controller is quite robust and has the fast dynamic response under the load change.

V. CONCLUSIONS

The characteristics and tendency of a P+MR controller are analyzed by observing the system change with the variation of each gain. An attempt is made to solve the voltage magnitude drop due to the practical PR control. Finally, the proposed method realized similar harmonics compensation performance

to the PI for harmonics compensation and analyzed how each gain variation of PR control affect the system bandwidth, stability, and resonant damping. Furthermore, the voltage magnitude drop due to the conventional practical PR control can be solved by using the PI-based simple voltage restoration method. The proposed method is verified through simulations and experiments. This research will be extended to the inner voltage controller of indirect current control for seamless mode transfer among both grid-connected and islanded mode [9], [10], [26]-[29].

ACKNOWLEDGMENT

This work was supported by the Korea Institute of Energy Technology Evaluation and Planning(KETEP) and the Ministry of Trade, Industry & Energy(MOTIE) of the Republic of Korea (No. 20168530050030).

REFERENCES

[1] *Distributed generation at Lawrence Berkeley National Laboratory* (LBNL), http://der.lbl.gov.
[2] *The Consortium for Electric Reliability Technology Solutions* (CERTS), http://certs.lbl.gov.
[3] *The GridWise alliance*, http://www.gridwise.org/.
[4] *Large Scale Integration of Micro-generation to Low Voltage Grids (MICROGRIDS)*, http://microgrids.power.ece.ntua.gr.
[5] *Distributed Intelligence in Critical Infrastructures for Sustainable Power* (CRISP), http://www.crisp.ecn.nl.
[6] *Distributed Generation with High Penetration of Renewable Energy Sources* (DISPOWER), http://www.dispower.org.
[7] K. Lim, J. Jang, J. Lee, J. Kim, and J. Choi, "P+ multiple resonant control for output voltage regulation of microgrid with unbalanced and nonlinear loads," in *Proc. of IPEC'2014 -ECCE Asia*,21G2-2, 2014.
[8] K. Lim, J. Jang, S. Moon, J. Kim, and J. Choi, "Output voltage regulation based on P plus resonant control in islanded mode of microgrids," in *Proc. of PEMC'2014*., pp. 452-457, 2014.
[9] J. Kwon, S. Yoon, and S. Choi, "Indirect current control for seamless transfer of three-phase utility interactive inverters," *IEEE Trans. Power Electron*., Vol. 27, No. 2, pp. 773-781, Feb. 2012.
[10] S. Yoon, H. Oh, and S. Choi, "Controller design and implementation of indirect current control based utility-interactive inverter system," *IEEE Trans. Power Electron*., Vol. 28, No. 1, pp. 26-30, Jan. 2013.
[11] D. De and V. Ramanarayanan, "A proportional + multi resonant controller for three-phase four-wire high-frequency link inverter," *IEEE Trans. Power Electron.*, Vol. 25, No. 4. pp. 899-906, 2010.
[12] D. De and V. Ramanarayanan, "Decentralized parallel operation of inverters sharing unbalanced and nonlinear loads," *IEEE Trans. Power Electron*, Vol. 25, No. 12. pp. 3015-3025, 2010.
[13] W. Yao, M. Chen, J. Matas, and J. M. Guererro. "Design and analysis of the droop control method for parallel inverters considering the impact of the complex impedance on the power sharing," *IEEE Trans. Ind. Electron*., Vol. 58, No. 2, pp. 576-588, Feb. 2011.
[14] K. Kim and D. Hyun, "Advanced synchronous reference frame controller for three-phase UPS powering unbalanced and nonlinear Loads," *Transactions of Korean Institute of Power Electronics (KIPE)*, Vol. 10, No. 5, pp. 508-517, 2005.
[15] H. Gu, X. Guo, and W. Wu, "Accurate power sharing control for inverter-dominated autonomous microgrid," in *Conf. Rec. of IPEMC' 2012-ECCE Asia*, pp. 368-372, 2012.
[16] Y. W. Li and C. N. Kao, "An accurate power control strategy for power-electronics-interfaced distributed generation units operation in a low voltage multi bus microgrid," *IEEE Trans. Power Electron*, Vol. 24, No. 12, pp. 2977-2988, Dec. 2009.
[17] J. C. Vasquez, J. M. Guerrero, M. Savaghebi, and R. Teodorescu, "Modeling, analysis, and design of stationary reference frame droop controlled parallel three-phase voltage source inverters," in *Proc. ICPE'2011-ECCE Asia*, pp. 272-279, 2011.
[18] F. Blaabjerg, R. Teodorescu, M. Liserre, and A. Timbus, "Overview of control and grid synchronization for distributed power generation system," *IEEE Trans. Ind. Electron.,* Vol. 53, No. 5, pp. 1398-1409, Oct. 2006.
[19] D. N. Zmood, D. G. Holmes, and G. H. Bode, "Stationary frame current regulation of PWM inverters with zero steady-state error," *IEEE Trans. Power Electron*, Vol. 18, No. 3, pp. 814-822, May 2003.
[20] Y. Sato, T. Ishizuka, K. Nezu, and T. Kataoka, "A new control strategy for voltage-type PWM rectifiers to realize zero steady-state control error in input current," *IEEE Trans. Ind. Application*., Vol. 34, No. 3, pp. 480-486, May/Jun. 1998.
[21] W. Feng, K. Sun, Y. Guan, J. M. Guerrero, and X. Xiao, "The frequency fluctuation impact analysis for droop controlled grid-connecting inverter in microgrid," in *Proc. of IPEMC'2016- ECCE Asia*, 2016.
[22] Y. Guan, J. C. Vasquez, and J. M. Guerrero, "Hierarchical controlled grid-connected microgrid based on a novel autonomous current sharing controller," in *Proc. of ECCE'2015- ECCE Asia*, pp. 2333-2340, 2015.
[23] A. Micallef, M. Apap, C. Spiteri-Staines, J. M. Guerrero, and J. C. Vasquez, "Reactive power sharing and voltage harmonic distortion compensation of droop controlled single phase islanded microgrids," *IEEE Trans. Smart Grid*, Vol. 5, No. 3, pp. 1149-1158, May 2014.
[24] T. Ye, N. Y. Dai, and C. S. Lam, "Analysis, design, and implementation of a quasi-proportional-resonant controller for a multiplication capacitive-coupling grid-connected inverter," *IEEE Trans. Ind. Application*., Vol. 52, No. 5, pp. 4269-4279, Sep./Oct. 2016.
[25] F. G. Espin, I. Patrao, and E. Figueres, "An adaptive digital control technique for improved performance of grid connected inverters," *IEEE Trans. Ind. Inform.,* Vol. 9, No. 2, pp. 708-718, May 2013.
[26] T. Hornik, *Power Quality in Microgrids*, Ph. D. Dissertation, University of Liverpool, U.K., 2010.
[27] Z. Liu, J. Liu, and Y. Zhao, "A Unified control strategy for three-phase inverter in distributed federation," *IEEE Trans. Power Electron*, Vol. 29, No. 3, pp. 1176-1191, Mar. 2014.
[28] Z. Liu and J. Liu, "Indirect current control based seamless transfer of three-phase inverter in distributed generation," *IEEE Trans. Power Electron*., Vol. 29, No. 7, pp.3368-3383, Jul. 2014
[29] K. Lim and J. Choi, "PR based indirect current control for seamless transfer," in *Conf. Rec. of IPEMC'2016-ECCE Asia*, 2016.

Kyungbae Lim was born in Cheongju, Korea. He received his B.S. and M.S. degrees from the School of Electrical Engineering, Chungbuk National University, Cheongju, Korea, in 2011 and 2013, respectively, where he is presently working towards his Ph.D. degree. His current research interests include parallel operation, harmonic compensation and seamless mode transfer for DG based Microgrid operation.

Jaeho Choi received his B.S., M.S., and Ph.D. degrees from the Department of Electrical Engineering, Seoul National University, Seoul, Korea, in 1979, 1981, and 1989, respectively. From 1981 to 1983, he was with the Jungkyoung Technical College, Daejeon, Korea, as a full-time Lecturer. Since 1983, he has been with the School of Electrical Engineering, Chungbuk National University, Cheongju, Korea, where he is presently a Professor. In 1993, 1998, 2003, and 2009 he was a Visiting Professor at the University of Toronto, Toronto, Canada. He was also a Danfoss Visiting Professor at Aalborg University, Aalborg, Denmark, in 2000. His current research interests include power electronics, power quality problems and solutions, energy storage systems, and renewable energy and microgrid systems. He is an active Member of the KIEE, KIPE, and IEEE. He was the Editor-in-Chief of the JPE and the President of the KIPE.